Integrated in Clothes Graphene Antenna with Low SAR for Wearable Body-Centric Communications

T. N. Kapetanakis [1], C. D. Nikolopoulos [1, 2], C. Petridis [1], I. O. Vardiambasis[1*]

[1] Department of Electronic Engineering
Hellenic Mediterranean University, HMU
Romanou 3, Chalepa, Chania, Crete, 73133
Greece

[2] School of Electrical and Computer Engineering,
National Technical University of Athens, NTUA,
Iroon Polytechneiou 9, 15780
Athens, Greece

Received: April 15, 2021. Received: October 3, 2021. Accepted: November 1, 2021. Published: November 17, 2021.

Abstract— The design and fabrication of graphene based textile patch antennas, intended for use in the 2.45GHz ISM band, are presented. The antennas have simple geometries with rectangular, triangular, or circular shape and substrate materials made of four different fabrics suitable for wearable applications. Conductive graphene sheet is used for the active element patches of the twelve different proposed prototypes. The effects of the antenna geometry, the substrate selection and the graphene-textile fabrication process on the prototypes' performance are studied. Several prototypes exhibit desirable characteristics, such as high gain, acceptable radiation pattern, low Specific Absorption Rate (SAR), relatively wide bandwidth, and coverage of the ISM band even under different bending conditions.

Keywords— graphene antenna, textile antenna, patch antenna, wearable antenna, low SAR antenna, curved antenna, Internet of Things.

I. INTRODUCTION

BODY - centric communications are at the core of modern state of the art commercial and military applications such as medical, healthcare, personal entertainment, sport activities, and tactical communications. The human's body oriented approach (within, around, and upon) attracted the attention of many researchers and research resources over the years and still experiences increasing growing [1]–[3]. The above mentioned antennas have to embedded to clothes and should be flexible, comfortable and stretchable in order to be able to suit on curvilinear surfaces and endure dynamic motions [4]–[6].

Due to the increasing research interest of flexible conductive materials, new antenna designs have been developed and embedded on wearable electronic devices. These components are becoming advantageous in the field of wearable technology with the old rigid materials such as copper tend to be replaced. Especially, the demanding of flexible electronic devices from the IoT industry make wearable antennas to a great extent necessary for uninterrupted and unobstructed communication and transmission of information between nodes and humans [3], [4], [6], [7].

Wearable antennas due to their compact size, flexibility, and light weight can be easily embedded into clothes. These unique characteristics make them valuable in body-centric communications in order to smart interfaces and interaction between humans and technology to be established [6], [8]. On the other hand their design and fabrication is a challenging task in order their properties, specifications and advantages to be met [9]–[14].

Besides other frequency bands the Industrial Scientific & Medical (ISM) at 2.4 – 2.5 GHz is widely used for wearable applications. Typical example, the textile logotype wearable antennas which proposed in [15], [16] while a number of flexible antennas are presented in [17]–[21] for a variety of body-centric applications.

A number of different shapes and structures of wearable and textile antennas have been suggested and fabricated recently by research community. The relative literature is extensive. To mention a few, [22] realizes an embroidered metamaterial antenna for RFID applications, [15] implements logo-type colorful wearable antennas, [23] proposes a folded rectangular half-mode substrate-integrated cavity antenna, [24] presents a textile antenna consisting of a circular ring slot on a substrate integrated waveguide cavity-feed structure, [25], [26] constructs a mixed embroidered-woven textile integrated waveguide antenna, [27] reports a dipole antenna on the Kapton polyimide substrate for flexible display devices, [28] fabricates a slotted patch antenna on e-textile created with sewed copper tape, [29] fabricates an embroidered meander ring dipole antenna, [30] introduces cotton or denim substrates to slit loaded textile antennas, and [10], [11] embroider fractal bowtie antennas.

On the other hand, microstrip patch antennas of various geometries, due to their compact size, light weight, low profile, planar configuration, easy fabrication, convenient modularization, high reliability, simple integrability with solid state devices, and low cost, are important in both theoretical research and engineering applications and widely used as transmitting antennas, despite in some cases their limited usable frequency bandwidth and low gain [26], [31].

Perhaps, wearable electronics are recognized as one of the hottest topics in today's research community. Recent trends tend to replace traditional rigid metallic materials such as copper with innovative materials such as graphene, the allotrope of carbon nanotube [32]. The great research interest in materials science led to use graphene as a very promising material for the design and fabrication of RF, microwave, and millimeter wave devices [33]. Especially the improvements of the electrical conductivity in combination with its light weight (around 5 times than copper [34]), structure stability and mechanical flexibility make it one of the most efficient materials for flexible antennas. Zhang et al. [35] proposes a UHF RFID tag antenna based on high conductivity graphene assembly film (GAF), which can achieve a comparable performance of commercially available metallic antennas. Kumar et al. [36] presents a frequency reconfigurable microstrip antenna for satellite communications. The multilayer antenna designed and fabricated from graphene conductive ink printed textile as an alternative of metals after the experimental comparison with a traditional cooper based antenna. Lamminen et al. [37] suggests an UWB elliptical quasi dipole antenna measured in the frequency range from 1 GHz to 5 GHz. The antenna screen printed onto kapton substrate where the gain was measured 2 dBi at 2 GHz and the flexibility test shown a stable resistance after numerous bending cycles. Wang et al. [38] used water transfer method in order to fabricate graphene-based antenna printed on water-transferable paper substrate with a maximum gain of 0.7 dBi and 8.9% fractional bandwidth. Among the aforementioned graphene antennas flexible materials used as substrate (Kapton, photopaper, etc), herein is suggested graphene as conductive material in various geometries embedded on substrates of commercial available fabrics that are widely used in clothing industry.

II. Antenna design

The rectangular wearable under study antenna's geometry is depicted in Fig. 1. The structure of a rectangular microstrip patch, which is probe fed, consists of 5 layers: (i) the upper layer rectangular conductive patch (implemented of graphene paper) with thickness h_p, width W_p and length L_p, (ii) the very thin bonding layer (double-sided thermoplastic adhesive), attaching the substrate and patch textiles, with thickness ~10μm, width W_p and length L_p, (iii) the middle layer dielectric substrate (made of denim D1, denim D2, felt F1, or felt F2 textile) with thickness h_s, width W and length L, (iv) once again the very thin layer, now bonding the substrate and the ground plane, with thickness ~10μm, width W and length L, and (v) the bottom layer ground plane (implemented of the same material as the upper layer) with thickness h_p, width W and length L.

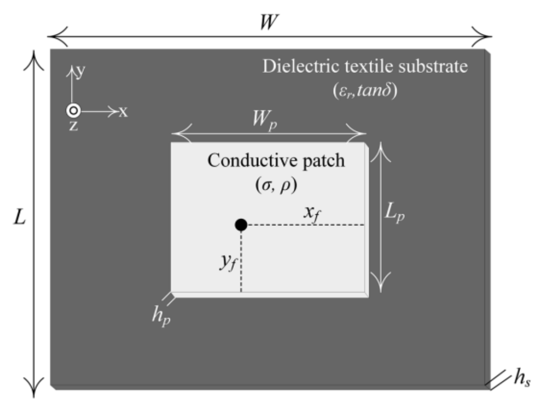

Fig. 1. The rectangular patch antenna geometry.

The design of textile rectangular patch antennas for the 2.45 GHz band, when the dielectric substrate's and the conducting active element's materials are known, is a two-stage procedure: (i) the initialization phase, when we determine the initial approximate dimensions of the microstrip resonating at 2.45 GHz using the transmission-line model [39], and (ii) the optimization phase, when the genetic algorithm tool of CST 2021 [40] evolves the initial dimensions to their optimal exact values.

Practical values of the length L_p and the width W_p of the rectangular microstrip antenna, ensuring adequate radiation efficiency, are given by [39]

$$L_p = \frac{1}{2 f_r \sqrt{\varepsilon_{ref} f} \sqrt{\varepsilon_0 \mu_0}} - 2\Delta L \tag{1}$$

$$W_p = \frac{1}{2 f_r \sqrt{\varepsilon_0 \mu_0}} \sqrt{\frac{2}{\varepsilon_r + 1}} \tag{2}$$

where ε_0 is the dielectric permittivity of free space, μ_0 the magnetic permeability of free space, ε_r the substrate's dielectric constant, f_r the frequency of resonance, ε_{reff} the microstrip antenna's effective dielectric constant

$$\varepsilon_{reff} = \frac{\varepsilon_r + 1}{2} + \frac{\varepsilon_r - 1}{2} \left[1 + 12 \frac{h_s}{W_p} \right]^{-1/2} \tag{3}$$

$$\frac{\Delta L}{h_s} = 0.412 \frac{\left(\varepsilon_{reff} + 0.3\right)\left(\frac{W_p}{h_s} + 0.264\right)}{\left(\varepsilon_{reff} - 0.258\right)\left(\frac{W_p}{h_s} + 0.8\right)} \tag{4}$$

and h_s the substrate's height.

The microstrip is fed by a below probe at (x_f, y_f), as shown in Fig. 1. The feed location is very significant for the input impedance, but it does not affect the resonant frequency very much. The distances x_f and y_f from the center of the microstrip are approximately given by [39]

$$x_f = \frac{W_p}{\pi} \sin^{-1} \sqrt{\frac{R_{in}}{R_{ed}}}, \; y_f = \frac{L_p}{\pi} \sin^{-1} \sqrt{\frac{R_{in}}{R_{ed}}} \tag{5}$$

where R_{in} is the input resistance and R_{ed} is the input resistance at the edge. The impedance varies from 0 at the center to R_{ed} at the edge, so the feed location should be carefully positioned in order to achieve the desirable input impedance Z_{in}=50+j0 Ω. The microstrip is fed by bringing the center conductor of an SMA connector through a hole in the ground plane and substrate, and connecting it electrically to the designed patch feed-point.

The geometry of the triangular wearable antenna is depicted in Fig. 2, where the triangular microstrip patch is a structure the same 5 layers as before. Now, the previous rectangular upper layer patch and rectangular bonding layer adhesive of Fig. 1 are replaced by the isosceles triangular conductive patch with base length W_p and height L_p, and an equal triangular adhesive layer, respectively.

In the initialization phase of the triangular case, we apply again the transmission line model values of the corresponding rectangular patch resonating at 2.45 GHz, and using equations (1) and (2) we determine the approximate height L_p and base length W_p of the triangular microstrip. As indicated in Fig. 2, the microstrip is fed by an SMA connector from underneath at x_f ; the distance of the feed point from the triangular antenna top which is approximately given by (5).

The geometry of the circular wearable antenna is shown in Fig. 3, where a probe fed circular microstrip patch is illustrated as a structure of the same 5 previous layers. Here, the triangular upper layer patch and the triangular adhesive layer of Fig. 2 are replaced by a circular conductive patch of diameter D, and an equal circular adhesive layer, respectively.

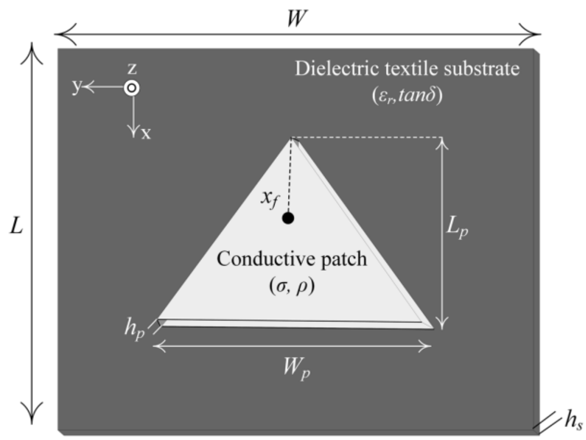

Fig. 2. The triangular patch antenna geometry.

The diameter D of a circular microstrip antenna [39], which is practically designed, is given by

$$D = \frac{0.02F}{\sqrt{1 + \frac{2h_s}{\pi \varepsilon_r F}\left(\ln\left(\frac{\pi F}{2h_s}\right) + 1.7726\right)}}, \quad F = 10^{11} \frac{8.791}{f_r \sqrt{\varepsilon_r}} \tag{6}$$

where ε_r is the dielectric constant of the substrate, h_s is the height of the substrate, and f_r is the resonant frequency.

With correspondence to the rectangular patch case, we use equation (5) to approximate the distances x_f and y_f of the feeding point from the microstrip center.

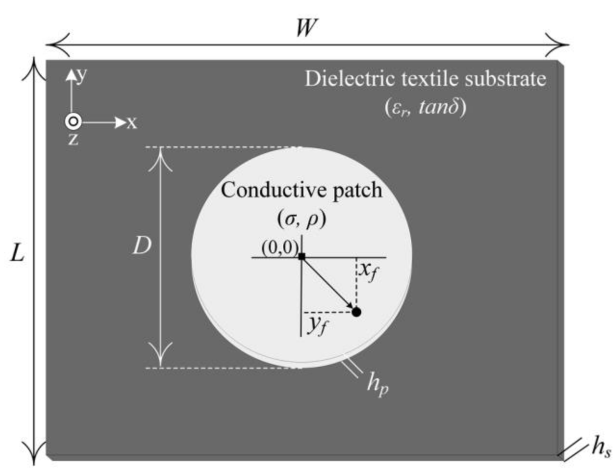

Fig. 3. The circular patch antenna geometry.

Next, during the optimization phase, a genetic algorithm is used to evolve the initial dimensions to their exact optimal values. Aiming to design textile patch antennas for the 2.45 GHz frequency band and to incorporate graphene in the design and fabrication process, we initialize the procedure by using parameters taken from equations (1)-(6) for the antennas' microstrip counterparts. The optimum values for the dimensions and the feeding point are finally given by the CST-2021's optimization tool [40]. The final design parameters' values are presented in the Section III for several different antenna prototypes.

III. Optimized Prototypes

The approximate values resulting from equations (1)-(6) are the initial estimations given to the optimization genetic algorithm of the CST software [40], in order to achieve for each under study patch antenna its final optimized geometrical characteristics that will be used for simulation and fabrication. In each case the exact material properties of the patch, the substrate and the ground-plane are taken into account or properly modeled. Characteristically, graphene-sheet modeled on CST Studio Suite [40] as ohmic sheets in order to relate the electromagnetic fields on their ohmic sheet surface. The unknown conductivities are modeled as impedance surfaces $Z_s=R_s+jX_s$, where both reactance X_s and resistance R_s are material properties. The impedance surface of graphene-sheet (conductive-fabric) is modeled as $Z_{s,Gs}= 0.338+j2.75$ ($Z_{s,Tc}= 0.35+j1.25$) @2.45GHz, as a result of an iterative method combining simulations and measurements [9], [41], [42].

TABLE I
Rectangular patch antenna's simulation and fabrication geometrical characteristics

Antenna prototype	RD1	RD2	RF1	RF2
Substrate Material	D1	D2	F1	F2
Patch Length L_p (mm)	44.0	41.6	51.5	48.5
Patch Width W_p (mm)	53.0	51.7	59.3	56.6
Feeding point (x_f, y_f) (mm)	(3.8, 4.5)	(15.5, 4.2)	(6.7, 15.8)	(2.0, 13.2)
Substrate Length L (mm)	88.0	83.1	103.1	96.9
Substrate Width W (mm)	106.0	103.4	118.6	113.2

TABLE II
Triangular patch antenna's simulation and fabrication geometrical characteristics

Antenna prototype	TD1	TD2	TF1	TF2
Substrate Material	D1	D2	F1	F2
Patch Length L_p (mm)	48.8	44.4	58.5	56.5
Patch Width W_p (mm)	62.3	59.8	69.5	67.3
Feeding point x_f (mm)	18.5	12.1	28.7	27.6
Substrate Length L (mm)	97.5	88.8	117.0	113.0
Substrate Width W (mm)	124.6	119.5	139.0	134.6

The exact geometrical characteristics for the simulation and fabrication of all 12 prototypes are given in Tables I, II and III. Each prototype has a code name consisted of 2 parts: (i) the first symbol "R", "T", or "C" stands for the rectangular, triangular, or circular shape of the patch, respectively, and (ii) the second tag "D1", "D2", "F1", or "F2" represents the 14oz thick denim, the 11oz thin denim, the polyester thick felt, or the wool thin felt textile of the substrate, respectively. In each case the patch and substrate materials, lengths and widths, as well as the feeding point position are listed in Tables I, II and III. In all cases the patches are made of graphene paper [43].

TABLE III
Circular patch antenna's simulation and fabrication geometrical characteristics

Antenna prototype	CD1	CD2	CF1	CF2
Substrate Material	D1	D2	F1	F2
Patch Diameter D (mm)	52.8	50.1	55.3	48.6
Feeding Point (x_f, y_f) (mm)	(15.5, 10.8)	(21.3, 1.2)	(20.5, 7.0)	(21.6, 2.6)
Substrate Length L and Width W (mm)	158.3	150.4	165.9	145.7

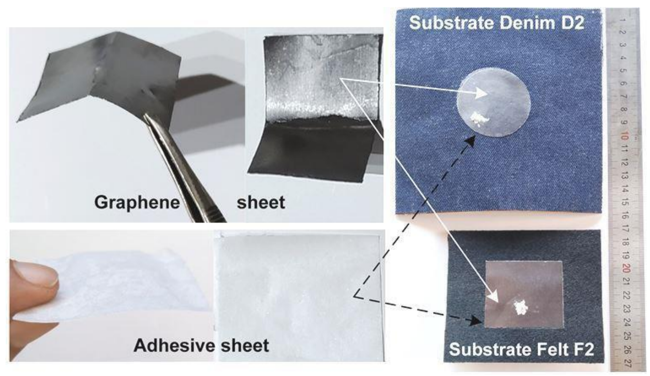

Fig. 4. The fabrication process for the patch antennas, made of graphene paper, on any substrate textile.

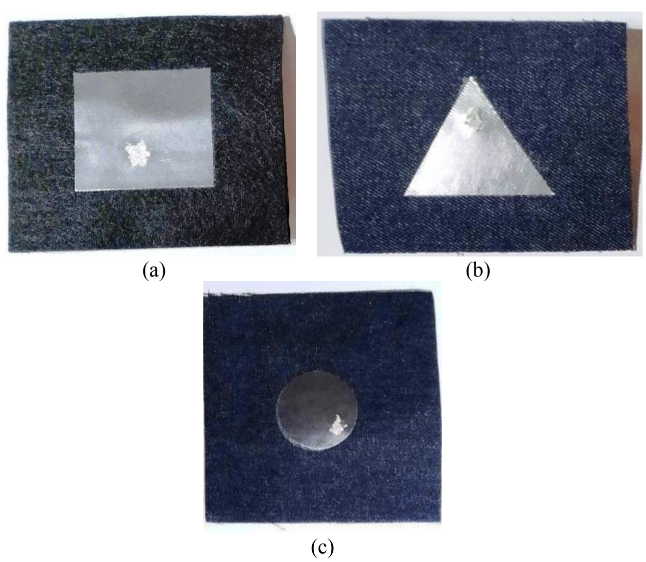

Fig. 5. Photographs of the fabricated patch antenna prototypes. (a) Rectangular RF2, (b) Triangular TD1, and (c) Circular CD1 patch.

The performance optimization @ 2.45 GHz of the 12 prototypes of Tables I, II and III results in dimensions that differ in all cases, because each one is characterized by a unique combination of patch shape, patch material, and substrate material.

All antenna prototypes have been fabricated by using a double sided thermoplastic adhesive to bond each conductive patch with the corresponding dielectric substrate. The fabrication procedure is graphically presented in Fig. 4.

The graphene-sheet and the adhesive-sheet are cut precisely to the optimized dimensions of a rectangular, triangular or circular patch using a CO_2 BRM laser 150 Watt, and permanently attached using thermal transfer method (due to the ultra-thin bonding-layer adhesive) upon the corresponding textile substrate previously cut to the appropriate size. Pictures of rectangular, triangular and circular fabricated prototypes, named RF2, TD1, and CD1 in Tables I, II and III, are presented in Fig. 5 (a)-(c). The characteristic stamp on every patch corresponds to the position of antenna feeding.

When it comes to the interconnection between wearable antennas, mobile devices and Internet of Things (IoT) nodes, several solutions can be proposed. In this work we use SMA connectors, because of the feasibility of conventional welding methods, while the usage of UFL and FME connectors would be equally effective. Other ways to feed and connect textile antennas could be either the usage of printed or embroidered textile transmission lines, or the embedance of the antenna and the portable device into a fully wearable PCB [10], [11], [15].

IV. Results

Firstly, measurements in free space under usual indoor environmental conditions (temperature 23°C and humidity 70%), were conducted for all prototypes. Table IV summarizes the measured characteristics of the prototypes, as well as the corresponding simulation results. The resonant frequency f_c, the magnitude of S_{11} and the Voltage Standing Wave Ratio (VSWR) at f_c are listed in the first 3 lines of Table IV, respectively. The -10dB bandwidth (BW) is given in the last two lines, while f_1 and f_2 stand for the lower and upper limit, respectively, of the aforementioned BW.

TABLE IV
Measured and simulated characteristics of selected antenna prototypes in free space

Antenna prototype	RF1	TD1	CD1	CF1
f_c (MHz) Simulated	2450	2450	2451	2433
f_c (MHz) Measured	2464	2446	2443	2457
S_{11} (dB) @ f_c Simulated	-55.4	-53.0	-45.5	-29.6
S_{11} (dB) @ f_c Measured	-19.47	-19.54	-18.79	-18.57
VSWR @ f_c Simulated	1.003	1.004	1.011	1.068
VSWR @ f_c Measured	1.2376	1.2355	1.2598	1.2672
f_1 (MHz) Simulated	2373	2364	2357	2380
f_1 (MHz) Measured	2389	2373	2363	2404
f_2 (MHz) Simulated	2532	2542	2552	2511
f_2 (MHz) Measured	2530	2539	2513	2521
BW (MHz) Simulated	159	178	195	131
BW (MHz) Measured	154	150	162	109
BW (%) Simulated	6.5	7.3	8.0	5.4
BW (%) Measured	6.3%	6.1%	6.6%	4.4%

The first remark about Table IV is that all prototypes cover the unlicensed 2.45 GHz ISM band, albeit the prototypes' performance may vary, depending on their fabrication, geometrical and material characteristics. It can be observed that all prototypes are close to the ISM's center frequency $f_{c,ISM}$ and the deviation Δf between the $f_{c,ISM}$ and the prototype's measured resonant frequency f_{cmeas}, calculated using (7), is less than 1%.

$$\Delta f = \frac{f_{csim} - f_{c,ISM}}{f_{csim}}, \quad f_{c,ISM} = 2450\,MHz \tag{7}$$

$$\Delta BW = \frac{BW_{sim} - BW_{meas}}{BW_{sim}} \tag{8}$$

On the other hand, the maximum bandwidth appears in the case of the circular patch CD1 prototype where the measured BW_{meas} =162 MHz. The deviation ΔBW between the simulated bandwidth BW_{sim} and the measured bandwidth BW_{meas}, calculated using (8), varies from 3% to 17%. Additionally, the minimum (maximum) deviation ΔBW appears in case of the rectangular (circular) patch prototype RF1 (CD1) prototype.

Fig. 6 presents the simulated and measured return loss, or in other words the S_{11} parameter, versus frequency for different patch antenna geometries on several textile substrates. It can be observed that all prototypes cover the whole 2.4 GHz ISM band, regardless of the geometry and the type of the substrate. In particular the RF2 prototype presents the simulated and measured resonant frequency f_{csim}= 2442 MHz and f_{cmeas}= 2439 MHz, respectively, which are in close agreement. In terms of simulated and measured bandwidth BW_{sim}= 124 MHz and BW_{meas}= 101 MHz, which are also in close agreement with less than 20% deviation.

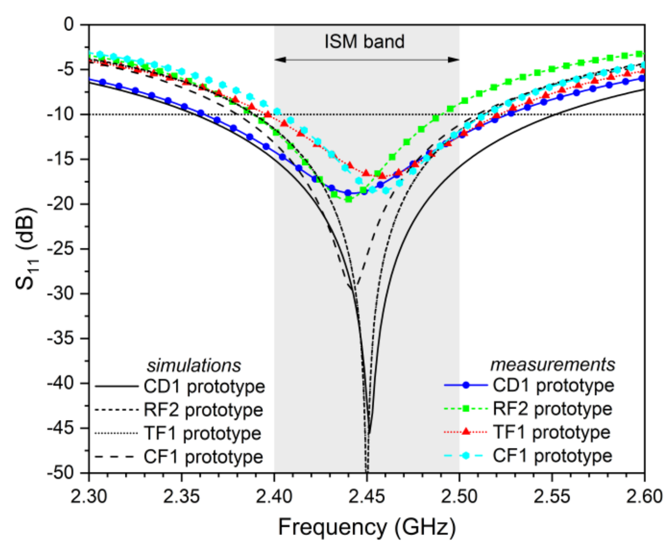

Fig. 6. Simulated and measured return loss (S_{11}) versus frequency of several prototypes.

On the other hand, the TF1 prototype presents the simulated and measured resonant frequency f_{csim}= 2450 MHz and f_{cmeas}=

INTERNATIONAL JOURNAL OF CIRCUITS, SYSTEMS AND SIGNAL PROCESSING
DOI: 10.46300/9106.2021.15.179 Volume 15, 2021

2459 MHz, respectively, which are in close agreement. The simulated and measured bandwidth BW_{sim}= 127 MHz and BW_{meas}= 124 MHz are also in close agreement with less than 1% deviation.

A. Performance under Bending Conditions

The performance of the antennas has been investigated under bending conditions. A representative illustration, of a circular patch antenna bent (convex) under y-axis is shown in Fig. 7(a), and the corresponding bent of a rectangular patch antenna bent (convex) under x-axis is shown in Fig. 7(b).

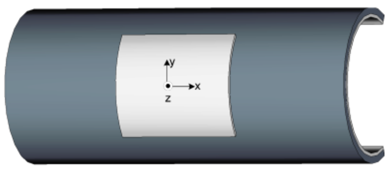

(a)

(b)

Fig. 7. Circular patch antenna under: (a) y-axis, and (b) x-axis bending.

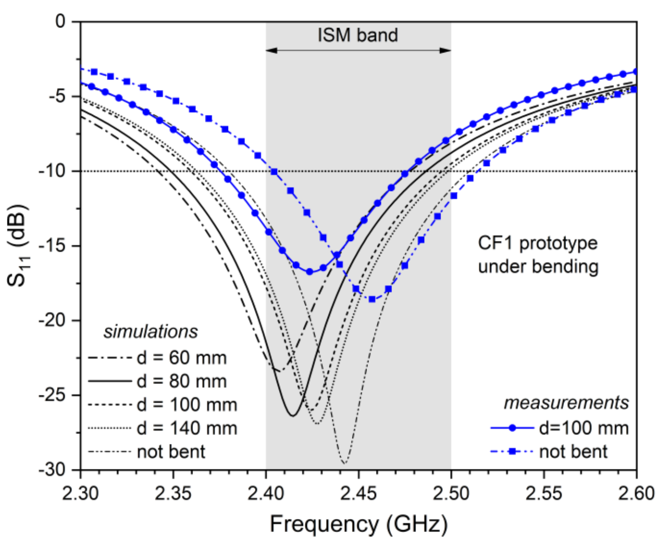

Fig. 8. Simulated and measured return loss (S_{11}) versus frequency for the CF1 prototype. The antenna is bent as shown in Fig. 7b.

In order to investigate the antennas under bending conditions the prototypes were mounted on a PVC cylindrical tubes (ε_r=4) and thickness 3 mm, with diameters d= 60, 80, 100, and 140 mm from the ground plane side (convex). The magnitude of S_{11} is plotted in Fig. 8, when the antenna is bent in a convex manner, along x-axis. The curves with markers depict the measured results and the curves without markers the corresponding simulated ones.

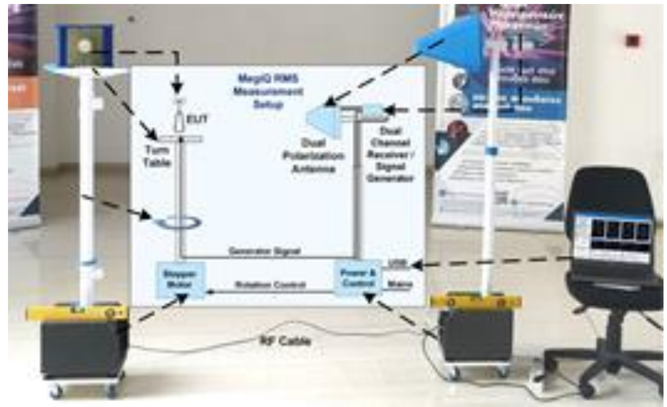

Fig. 9: Antenna radiation characteristics' measurement set-up. The antenna prototype is mounted on the rotary table on the left.

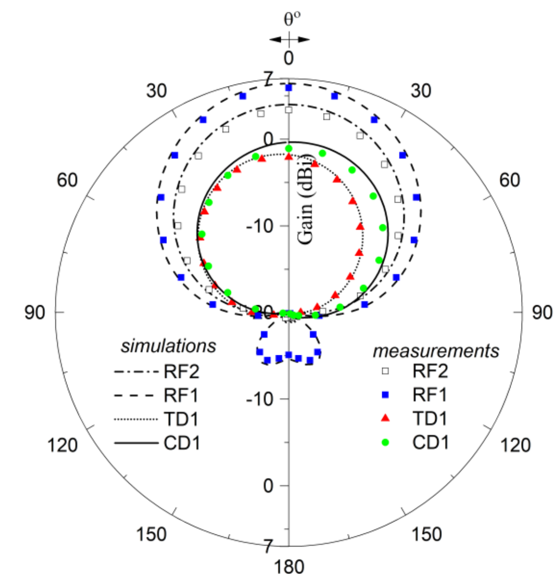

(a)

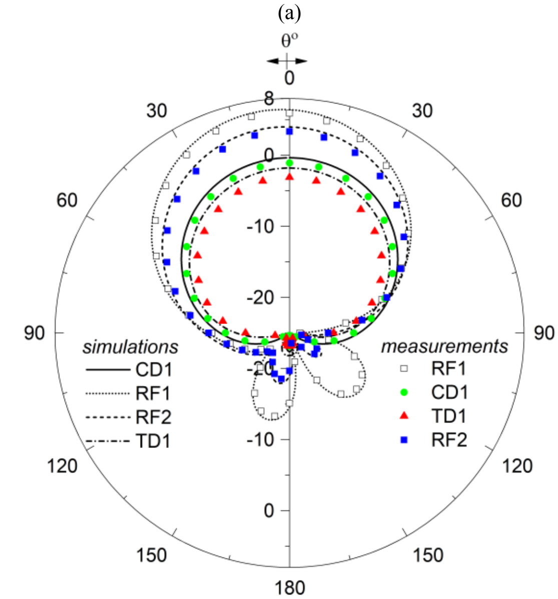

(b)

Fig. 10. Simulated (dotted, dashed and solid curves) and measured (circle, square and triangle symbols) free-space E-plane (θ- or elevation- plane) radiation patterns for the 4 prototypes referred to in each inset, when (a) φ=0° and (b) φ=90°.

Additionally the measured S_{11} is included as a reference and comparison to the not bent situation. From Fig. 8 it can be observed that during bending on a tube with diameter d=100 mm, the measured resonant frequency slightly shifts 33 MHz from 2457 MHz to 2424 MHz and the bandwidth decreases 7 MHz. On the other hand depending on the bending diameter d, the simulated resonant frequency slightly shifts 36, 28, 18, and 15 MHz, for d= 60, 80, 100, and 140 mm, respectively.

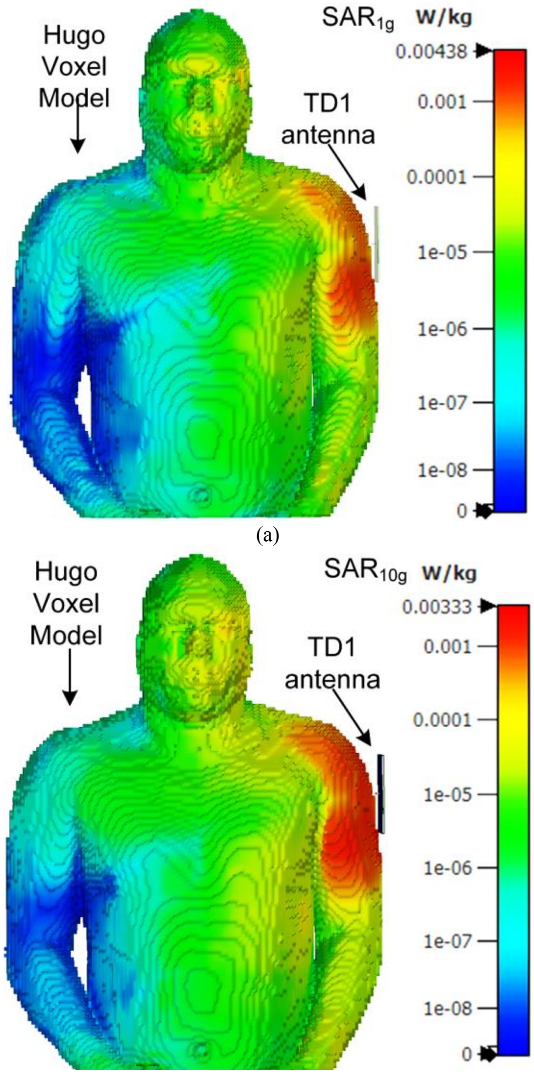

(a)

(b)

Fig. 11. SAR distribution for TD1 antenna prototype averaged for 1g (on the left) and 10g (on the right) of tissue.

The radiation characteristics of the fabricated herein prototypes were simulated using the CST software and measured using the antenna radiation measurement system MegiQ RMS-0660 [44], with the complete measurement set-up shown in Fig. 9.

The patch shape, the patch material and the substrate material significantly affect the prototypes' radiation characteristics. Indicative results are shown in Fig. 10. The solid and dashed curves depict simulated results, whereas the squares and circles correspond to the measured radiation patterns. Figs. 10(a) and 10(b) reveal a close agreement between simulated and measured results. Rectangular RF1 and RF2 patches present the highest measured and simulated gain, due to the low dielectric losses of the substrates. On the other hand, the triangular patch TD1 prototype presents the lowest gain, because of the denim substrate disadvantage in comparison to the CD1 prototype.

The simulated gain of the RF1, CD1, TD1, and RF2 prototypes is 6.49, -0.323, -1.69, and 4.00 dBi, respectively, while the measured gain of the same prototypes is 5.98, -1.07, -2.00, and 3.35 dBi, respectively.

B. SAR Estimation

Wearable antennas naturally are in close proximity to the human body, so it is necessary to perform an evaluation of a key parameter such as the Specific Absorption Rate (SAR). The exposure and electromagnetic absorption limits are determined by the regional regulating standards. A SAR limit value of 1.6 W/Kg (2 W/Kg) averaged per 1g (10g) of tissue has been determined for the general public in USA (EU) [45], [46]. Fig. 11 illustrates the SAR distribution (W/Kg) for TD1 prototype. The maximum values are observed in the arm area near the antenna location. As the distance from the prototype increases, SAR decreases. The SAR values do not exceed the general public regulation levels in any case. Their very low values may be attributed to the presence of the ground-plane layer.

TABLE V
MAXIMUM SAR VALUES AVERAGED FOR 10G AND 1G OF TISSUE FOR VARIOUS ANTENNA PROTOTYPES ACCORDING TO THE VOXEL MODEL

Antenna	SAR 10 g (W/Kg)	SAR 1 g (W/Kg)
RF1	0.011	0.016
CD2	0.002	0.003
CF1	0.003	0.004
TF1	0.003	0.004
TF2	0.002	0.003

V. CONCLUSION

Graphene based antennas, operational in the 2.45 GHz ISM band and easily embedded in clothing have been proposed in this paper. Rectangular, triangular, and circular antenna prototypes are simulated, optimized, fabricated, measured, and compared.

The evaluation of the proposed prototypes' performance has been examined through extensive simulations and measurements. The full coverage of the ISM band 2.40 GHz - 2.50 GHz is realized with simple antenna geometries, which at the same time satisfy their wearable character.

Several remarkable antenna performance characteristics, such as flexibility, simplicity, light weight, mechanical stability, bending, low cost, low SAR values and industry compatible fabrication process, can be mentioned.

However the conventional and not flexible SMA connection between the antenna and the transceiver module could be mentioned as a fabrication drawback. Also, the low under bending performance of the triangular prototypes should be reported. On the other hand, the results for the rest prototypes indicate acceptable performance (BW, gain etc.), with some of them being more promising. Regarding SAR, all prototypes are far below the exposure limits and thus can be effectively used for wearable IoT applications.

ACKNOWLEDGMENT

This research is co-financed by Greece and the European Union (European Social Fund - ESF) through the Operational Program "Human Resources Development, Education and Lifelong Learning 2014-2020" in the context of the project "Smart microwave nanomaterial structures with applications in bodycentric communications and the Internet of Things (MIS 5048187)".

REFERENCES

[1] P.S. Hall and Y. Hao, *Antennas and Radio Propagation for Body-Centric Wireless Communications*, 2nd Edition. Artech House: London, U.K., 2012.

[2] S. Rao, N. Llombart, E. Moradi, K. Koski, T. Bjorninen, L. Sydanheimo, J.M. Rabaey, J.M. Carmena, Y. Rahmat-Samii, and L. Ukkonen, "Miniature implantable and wearable on-body antennas: towards the new era of wireless body-centric systems," *IEEE Antennas Propag. Mag.*, vol. 56, no. 1, pp. 271–291, Feb. 2014, doi: 10.1109/MAP.2014.6821799.

[3] H. Sun, Y. Hu, R. Ren, L. Zhao, and F. Li, "Design of pattern-reconfigurable wearable antennas for body-centric Communications," *IEEE Antennas Wirel. Propag. Lett.*, vol. 19, no. 8, pp. 1385–1389, Aug. 2020, doi: 10.1109/LAWP.2020.3002016.

[4] S.G. Kirtania, A.W. Elger, R. Hasan, A. Wisniewska, K. Sekhar, T. Karacolak, and P.K. Sekhar, "Flexible antennas: A review," *Micromachines*, vol. 11, no. 9, 847, pp. 1-13, Sep. 2020, doi: 10.3390/mi11090847.

[5] B. Almohammed, A. Ismail, and A. Sali, "Electro-textile wearable antennas in wireless body area networks: materials, antenna design, manufacturing techniques, and human body consideration—a review," *Text. Res. J.*, vol. 91, no. 5–6, pp. 646–663, Mar. 2021, doi: 10.1177/0040517520932230.

[6] C. Loss, R. Gonçalves, C. Lopes, P. Pinho, and R. Salvado, "Smart coat with a fully-embedded textile antenna for IoT applications," *Sensors*, vol. 16, no. 6, p. 938, Jun. 2016, doi: 10.3390/s16060938.

[7] H. Khaleel, *Innovation in Wearable and Flexible Antennas*. WIT Press, 2015.

[8] J. Lilja, P. Salonen, T. Kaija, and P. De Maagt, "Design and manufacturing of robust textile antennas for harsh environments," *IEEE Trans. Antennas Propag.*, vol. 60, no. 9, pp. 4130–4140, 2012, doi: 10.1109/TAP.2012.2207035.

[9] R. Salvado, C. Loss, R. Gonçalves, and P. Pinho, "Textile materials for the design of wearable antennas: A survey," *Sensors*, vol. 12, no. 11, pp. 15841–15857, Nov. 2012, doi: 10.3390/s121115841.

[10] T.N. Kapetanakis, M. Pavec, M.P. Ioannidou, C.D. Nikolopoulos, A.T. Baklezos, R. Soukup, and I.O. Vardiambasis, "Embroidered bow-tie wearable antenna for the 868 and 915 MHz ISM bands," *Electronics*, vol. 10, no. 16, 1983, pp. 1-14, Aug. 2021, doi: 10.3390/electronics10161983.

[11] M. Pavec, T.N. Kapetanakis, M.P. Ioannidou, C.D. Nikolopoulos, A.T. Baklezos, R. Soukup, T. Blecha, and A. Hamacek, "Implementation of an all-textile bow-tie antenna for the 868 MHz ISM band," in *2020 International Symposium on Electromagnetic Compatibility - EMC EUROPE*, 2020, pp. 1–3, doi: 10.1109/EMCEUROPE48519.2020.9245778.

[12] A. Kiourti, C. Lee, and J. L. Volakis, "Fabrication of textile antennas and circuits with 0.1 mm precision," *IEEE Antennas Wirel. Propag. Lett.*, vol. 15, pp. 151–153, 2016, doi: 10.1109/LAWP.2015.2435257.

[13] A. Tsolis, W. Whittow, A. Alexandridis, and J. Vardaxoglou, "Embroidery and related manufacturing techniques for wearable antennas: Challenges and opportunities," *Electronics*, vol. 3, no. 2, pp. 314–338, May 2014, doi: 10.3390/electronics3020314.

[14] J. Zhong, C. W. Lee, D. Papantonis, A. Kiourti, and J.L. Volakis, "Body-worn 30:1 bandwidth tightly coupled dipole array on conductive textiles," *IEEE Antennas Wirel. Propag. Lett.*, vol. 17, no. 5, pp. 723–726, May 2018, doi: 10.1109/LAWP.2018.2803684.

[15] A. Kiourti and J.L. Volakis, "Colorful textile antennas integrated into embroidered logos," *J. Sens. Actuator Networks*, vol. 4, no. 4, pp. 371–377, Dec. 2015, doi: 10.3390/JSAN4040371.

[16] J. Tak and J. Choi, "An all-textile Louis Vuitton logo antenna," *IEEE Antennas Wirel. Propag. Lett.*, vol. 14, pp. 1211–1214, 2015, doi: 10.1109/LAWP.2015.2398854.

[17] A. Yadav, V. Kumar Singh, A. Kumar Bhoi, G. Marques, B. Garcia-Zapirain, and I. de la Torre Díez, "Wireless body area networks: UWB wearable textile antenna for telemedicine and mobile health systems," *Micromachines*, vol. 11, no. 6, 558, pp. 1-22, May 2020, doi: 10.3390/mi11060558.

[18] M. I. Ahmed, M. F. Ahmed, and A.-E. H. Shaalan, "SAR calculations of novel textile dual-layer uwb lotus antenna for astronauts spacesuit," *Prog. Electromagn. Res. C*, vol. 82, pp. 135–144, 2018, doi: 10.2528/PIERC18010911.

[19] R. Bharadwaj, S. Swaisaenyakorn, C. G. Parini, J. C. Batchelor, and A. Alomainy, "Impulse radio ultra-wideband communications for localization and tracking of human body and limbs movement for healthcare applications," *IEEE Trans. Antennas Propag.*, vol. 65, no. 12, pp. 7298–7309, Dec. 2017, doi: 10.1109/TAP.2017.2759841.

[20] V. K. Singh, S. Dhupkariya, and N. Bangari, "Wearable ultra wide dual band flexible textile antenna for WiMax/WLAN application," *Wirel. Pers. Commun.*, vol. 95, no. 2, pp. 1075–1086, Jul. 2017, doi: 10.1007/s11277-016-3814-7.

[21] Y. Gao, Y. Zheng, S. Diao, W.-D. Toh, C.-W. Ang, M. Je, and C.-H. Heng, "Low-power ultrawideband wireless telemetry transceiver for medical sensor applications," *IEEE Trans. Biomed. Eng.*, vol. 58, no. 3, pp. 768–772, Mar. 2011, doi: 10.1109/TBME.2010.2097262.

[22] M. A. Ziai and J. C. Batchelor, "Temporary on-skin passive UHF RFID transfer tag," *IEEE Trans. Antennas Propag.*, vol. 59, no. 10, pp. 3565–3571, Oct. 2011, doi: 10.1109/TAP.2011.2163789.

[23] F. X. Liu, Z. Xu, D. C. Ranasinghe, and C. Fumeaux, "Textile folded half-mode substrate-integrated cavity antenna," *IEEE Antennas Wirel. Propag. Lett.*, vol. 15, pp. 1693–1697, 2016, doi: 10.1109/LAWP.2016.2524458.

[24] Y. Hong, J. Tak, and J. Choi, "An all-textile SIW cavity-backed circular ring-slot antenna for WBAN applications," *IEEE Antennas Wirel. Propag. Lett.*, vol. 15, pp. 1995–1999, 2016, doi: 10.1109/LAWP.2016.2549578.

[25] S. Amendola, G. Bovesecchi, A. Palombi, P. Coppa, and G. Marrocco, "Design, calibration and experimentation of an epidermal RFID sensor for remote temperature monitoring," *IEEE Sens. J.*, vol. 16, no. 19, pp. 7250–7257, Oct. 2016, doi: 10.1109/JSEN.2016.2594582.

[26] J. A. Ansari, P. Singh, and N. P. Yadav, "Analysis of wideband multilayer patch antenna with two parasitic elements," *Microw. Opt. Technol. Lett.*, vol. 51, no. 6, pp. 1397–1401, Jun. 2009, doi: 10.1002/MOP.24378.

[27] M. T. Islam, T. Alam, I. Yahya, and M. Cho, "Flexible radio-frequency identification (RFID) tag antenna for sensor applications," *Sensors*, vol. 18, no. 12, 4212, pp. 1-9, Nov. 2018, doi: 10.3390/S18124212.

[28] O. El Maleky, F. Ben Abdelouahab, M. Essaaidi, and M. A. Ennasar, "Design of simple printed dipole antenna on flexible substrate for UHF band," *Procedia Manuf.*, vol. 22, pp. 428–435, Jan. 2018, doi: 10.1016/J.PROMFG.2018.03.067.

[29] B. Moradi, R. Fernández-García, and I. Gil, "Wearable high-performance meander ring dipole antenna for electronic-textile applications," *J Textile Instit.*, vol. 111, no. 2, pp. 178–182, Feb. 2019, doi: 10.1080/00405000.2019.1628886.

[30] R. Sreemathy, S. Hake, S. Sulakhe, and S. Behera, "Slit loaded textile microstrip antennas," *IETE J. Res.*, pp. 1-9, 2020, doi: 10.1080/03772063.2019.1709572.

[31] A.H. Abdelgwad, "Microstrip patch antenna enhancement techniques,"

Int. J. Electr. Electron. Commun. Sci., vol. 12, no. 10, pp. 703–710, 2018, doi: 10.5281/zenodo.1474773.

[32] J.J. Zhang, R. Song, X. Zhao, R. Fang, B. Zhang, W. Qian, J. Zhang, C. Liu, and D. He, “Flexible graphene-assembled film-based antenna for wireless wearable sensor with miniaturized size and high sensitivity,” *ACS Omega*, vol. 5, no. 22, pp. 12937–12943, Jun. 2020, doi: 10.1021/acsomega.0c00263.

[33] X. Huang, T. Leng, K. H. Chang, J. C. Chen, K. S. Novoselov, and Z. Hu, “Graphene radio frequency and microwave passive components for low cost wearable electronics,” *2D Mater.*, vol. 3, no. 2, 025021, May 2016, doi: 10.1088/2053-1583/3/2/025021.

[34] R. Song, Q. Wang, B. Mao, Z. Wang, D.Tang, B. Zhang, J. Zhang, C. Liu, D. He, Z. Wu, and S. Mu, “Flexible graphite films with high conductivity for radio-frequency antennas,” *Carbon*, vol. 130, pp. 164–169, Apr. 2018, doi: 10.1016/j.carbon.2018.01.019.

[35] B. Zhang, Z. Wang, R. Song, H. Fu, X. Zhao, C. Zhang, D. He, and Z.P. Wu, “Passive UHF RFID tags made with graphene assembly film-based antennas,” *Carbon*, vol. 178, pp. 803–809, Jun. 2021, doi: 10.1016/j.carbon.2021.02.096.

[36] J. Kumar, B. Basu, F. A. Talukdar, and A. Nandi, “Graphene- based multimode inspired frequency reconfigurable user terminal antenna for satellite communication,” *IET Commun.*, vol. 12, no. 1, pp. 67–74, Jan. 2018, doi: 10.1049/iet-com.2017.0253.

[37] A. Lamminen, K. Arapov, G. de With, S. Haque, H.G.O. Sandberg, H. Friedrich, and V. Ermolov, “Graphene-flakes printed wideband elliptical dipole antenna for low-cost wireless communications applications,” *IEEE Antennas Wirel. Propag. Lett.*, vol. 16, pp. 1883–1886, 2017, doi: 10.1109/LAWP.2017.2684907.

[38] W. Wang, C. Ma, X. Zhang, J. Shen, N. Hanagata, J. Huangfu, and M. Xu, “High-performance printable 2.4 GHz graphene-based antenna using water-transferring technology,” *Sci. Technol. Adv. Mater.*, vol. 20, no. 1, pp. 870–875, Dec. 2019, doi: 10.1080/14686996.2019.1653741.

[39] C.A. Balanis, *Antenna Theory: Analysis and Design,* 4th ed., John Wiley & Sons Inc., 2016.

[40] “CST Studio Suite electronagnetic field simulation software,” 2021. [Online]. Available: https://www.3ds.com/products-services/simulia/products/cst-studio-suite/.

[41] S. Sankaralingam and B. Gupta, “Determination of dielectric constant of fabric materials and their use as substrates for design and development of antennas for wearable applications,” *IEEE Trans. Instrum. Meas.*, vol. 59, no. 12, pp. 3122–3130, Dec. 2010, doi: 10.1109/TIM.2010.2063090.

[42] A.W. Memon, I.L. de Paula, B. Malengier, S. Vasile, P. Van Torre, and L. Van Langenhove, “Breathable textile rectangular ring microstrip patch antenna at 2.45 GHz for wearable applications,” *Sensors*, vol. 21, no. 5, 1635, pp. 1-17, Feb. 2021, doi: 10.3390/s21051635.

[43] “Sigma-Aldrich graphene paper XG Leaf” [Online]. Available: https://www.sigmaaldrich.com.

[44] “MegiQ radiation measurement system” [Online]. Available: https://www.megiq.com/products/rms-0460.

[45] IEEE, "Determining the peak spatial average specific absorption rate (SAR) in the human body from wireless communications devices, 30 MHz - 6 GHz. Part 1: General requirements for using the finite difference time domain (FDTD) method for SAR calculations," 2014.

[46] IEEE, “IEEE PC95.3 - IEEE Draft recommended practice for measurements and computations of electric, magnetic and electromagnetic fields with respect to human exposure to such fields, 0 Hz - 300 GHz,” 2016.

Author Contributions

Conceptualization, T.N.K. and I.O.V.; methodology, T.N.K. and I.O.V.; software, C.D.N.; validation, T.N.K., C.D.N., and I.O.V.; formal analysis, K.P. and I.O.V.; measurements, T.N.K. and C.D.N.; investigation, T.N.K., C.D.N., K.P. and I.O.V.; resources, C.D.N., T.N.K. and I.O.V.; data curation, C.D.N. and T.N.K.; writing original draft preparation, T.N.K., K.P. and I.O.V.; writing review and editing, T.N.K. and I.O.V.; visualization, C.D.N. and T.N.K.; supervision, I.O.V.; project administration, K.P. and I.O.V.; funding acquisition, T.N.K., K.P, C.D.N. and I.O.V.